

Intervention Generalization: A View from Factor Graph Models

Gecia Bravo-Hermsdorff^{1*}, David S. Watson², Jialin Yu¹,
Jakob Zeitler¹, and Ricardo Silva¹

¹University College London ²King's College London

*Corresponding author: g.hermsdorff@ucl.ac.uk

Abstract

One of the goals of causal inference is to generalize from past experiments and observational data to novel conditions. While it is in principle possible to eventually learn a mapping from a novel experimental condition to an outcome of interest, provided a sufficient variety of experiments is available in the training data, coping with a large combinatorial space of possible interventions is hard. Under a typical sparse experimental design, this mapping is ill-posed without relying on heavy regularization or prior distributions. Such assumptions may or may not be reliable, and can be hard to defend or test. In this paper, we take a close look at how to warrant a leap from past experiments to novel conditions based on minimal assumptions about the factorization of the distribution of the manipulated system, communicated in the well-understood language of factor graph models. A postulated *interventional factor model* (IFM) may not always be informative, but it conveniently abstracts away a need for explicit unmeasured confounding and feedback mechanisms, leading to directly testable claims. We derive necessary and sufficient conditions for causal effect identifiability with IFMs using data from a collection of experimental settings, and implement practical algorithms for generalizing expected outcomes to novel conditions never observed in the data.

1 Introduction

Causal inference is a fundamental problem in many sciences, such as clinical medicine [6, 52, 49] and molecular biology [45, 28, 21]. For example, causal inference can be used to identify the effects of chemical compounds on cell types [52] or determine the underlying mechanisms of disease [37].

One particular challenge in causal inference is *generalization* — the ability to extrapolate knowledge gained from past experiments and observational data to previously unseen scenarios. Consider a laboratory that has performed several gene knockouts and recorded subsequent outcomes. Do they have sufficient information to predict how the system will behave under some new combination(s) of knockouts? Conducting all possible experiments in this setting would be prohibitively expensive and time consuming. A supervised learning method could, in principle, map a vector representation of the design to outcome variables of interest. However, past experimental conditions may be too sparsely distributed in the set of all possible assignments, and such a direct supervised mapping would require leaps of faith about how assignment decisions interact with the outcome, even if under the guise of formal assumptions such as linearity.

In this paper, we propose a novel approach to the task of *intervention generalization*, i.e. predicting the effect of unseen treatments levels on an outcome of interest. We rely on little more than a postulated factorization of the distribution describing how intervention variables σ interact with a random process X to determine outcomes Y .

Related setups appear in the causal modeling literature on soft interventions [13], including its use in methods such as causal bandits [31] and causal Bayesian optimization [3] (see Section 6). However, these methods rely on directed acyclic graphical models (DAGs), which may be hard to justify. Without claiming that our proposal is appropriate for every application, we submit that simpler causal structures should be the starting point for intervention generalization. Our *interventional factor model* (IFM) leads to provable intervention generalization via a factor graph decomposition which, when informative, can be tested without further assumptions beyond basic relations of conditional independence. IFM is fully agnostic with regards to cycles or hidden variables, in the spirit of Dawid [17]’s decision-theoretic approach to causal inference, where the key ingredient boils down to statements of conditional independence among random and intervention variables.

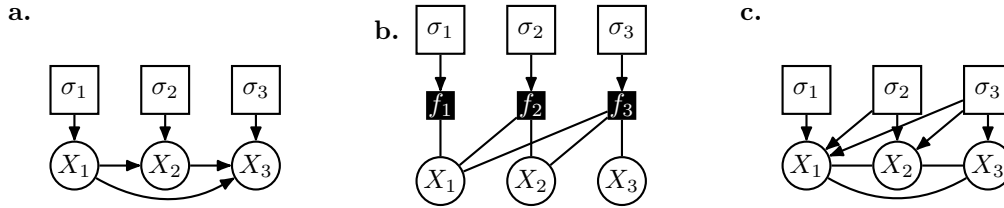


Figure 1: Three different causal graphical models, with explicit intervention vertices, expressing different factorization assumptions: **(a)** a directed acyclic graph (DAG); **(b)** a factor graph; and **(c)** a chain graph. Random variables are represented as circles, and intervention variables as squares.

Our primary contributions are as follows. (1) We introduce the *interventional factor model* (IFM), which aims to solve intervention generalization problems using only claims about which interventions interact with which observable random variables. (2) We establish necessary and sufficient conditions for the identifiability of treatment effects within the IFM framework. (3) We adapt existing results from conformal inference to our setting, providing distribution-free predictive intervals for identifiable causal effects with guaranteed finite sample coverage. (4) We implement our model using an efficient algorithm, and put it to use on a range of semi-synthetic experiments, where it successfully computes causal estimands in novel regimes.

2 Problem Statement

Background and notation. The notion of an *intervention* variable in causal inference encodes an action that modifies the distribution of a system of random variables. This notion is sometimes brought up explicitly in graphical formulations of causal models [41, 51, 17]. To formalize it, let σ denote a vector of *intervention variables* (also known as *regime indicators*), with σ_i taking values in a finite set $\{0, 1, 2, \dots, \aleph_i - 1\}$. From a graphical perspective, intervention variables will be depicted here using white square vertices with black labels; random variables will be represented as circles (Fig. 1). In a typical DAG formalism, such intervention nodes have no parents and point to at least one random variable.

Pearl’s *do* operator [41], for instance, denotes whether a particular random variable X_i is manipulated to have a value of (say) 0 by $do(X_i = 0)$, or 1 by $do(X_i = 1)$, and so on. This can be expressed by an intervention variable σ_i where $\sigma_i = 0$ is used to denote “no manipulation”, $\sigma_i = 1$ denotes “ $do(X_i = 0)$ ” and $\sigma_i = 2$ denotes “ $do(X_i = 1)$.”¹ Fig. 1(a) shows an example of a causal DAG with explicit intervention variables. In general, there is no need for intervention variables to have a one-to-one correspondence with random variables, nor to only represent the deterministic setting of random variables to fixed values, as operationalized by the *do* operator. They may in principle describe any well-defined change in distribution, e.g. stochastic or conditional interventions [17, 14].

At its most abstract level, the independence constraints encoded in a causal model do not need to correspond to a DAG. In fact, for many data generating processes, a DAG factorization is an artificial choice. For instance, in cell biology studies, data are collected at a design level σ by waiting for a stochastic process X to settle into equilibrium. Only then are samples collected. In this case, the probability density/mass function $p(x; \sigma)$ is the result of a feedback process that does not naturally fit a DAG representation. A growing literature in causal inference carefully considers how DAGs may give rise to equilibrium distributions (e.g., [9, 8]), but they come with considerable added complexity of assumptions to ensure identifiability.

We abstract away all low-level details about how an equilibrium distribution comes to be, and instead require solely a model for how a distribution $p(x; \sigma)$ factorizes as a function of σ . These assumptions are naturally formulated as a factor graph model [30] augmented with intervention variables, which is detailed in the next section. Such a structure can also come from DAG assumptions. In Fig. 1(b), we depict a variation of factor graphs [30], which we call an *interventional* factor graph, by adding a black vertex with white labels to denote factors corresponding to the DAG in Fig. 1(a), where $f_1(x_1; \sigma_1) := p(x_1; \sigma_1)$, $f_2(x_1, x_2; \sigma_2) := p(x_2 | x_1; \sigma_2)$ and $f_3(x_1, x_2, x_3; \sigma_3) := p(x_3 | x_1, x_2; \sigma_3)$. This explicitly represents that the conditional distribution of X_3 given all other (random and interventional) variables fully factorizes in

¹Intervention levels can generally be chosen from a space of uncountably many different values. However, for the identifiability results in the next section, it will pay to cover the finite case only, as it removes the need for smoothness assumptions on the effect of intervention levels. Also notice the slight abuse of notation to call $\sigma_i = 0$ an “intervention”, as it is convenient to treat the “natural” regime as just another choice of data generating process.

σ : i.e., $p(x_3 | x_1, x_2, \sigma) \propto f_1(x_1; \sigma_1) f_2(x_1, x_2; \sigma_2) f_3(x_1, x_2, x_3; \sigma_3)$. This factorization is not automatically enforced by usual parameterizations of Markov random fields (i.e., graphical models with only undirected edges) or chain graphs (graphical models with acyclic directed edges and undirected edges) [19], for which the corresponding chain graph (with interventions) for this example is shown in Fig. 1(c).

Problem statement. We are given a space Σ of possible values for an intervention vector σ of dimension d , making $|\Sigma| \leq \prod_{i=1}^d \aleph_i$. Each fully specified intervention vector characterizes a *regime* or an *environment* (we use these terms interchangeably). Given a range of training regimes $\Sigma_{train} \subset \Sigma$ and a random variable Y quantifying an event taking place after the choice of intervention, we want to learn $\mu_\sigma := \mathbb{E}[Y; \sigma]$ for all test environments $\sigma \in \Sigma_{test} = \Sigma \setminus \Sigma_{train}$.

We are also given collection of datasets $\mathcal{D}^1, \mathcal{D}^2, \dots, \mathcal{D}^t$, with dataset \mathcal{D}^j collected under environment $\sigma^j \in \Sigma$. We use Σ_{train} to denote the set $\{\sigma^1, \sigma^2, \dots, \sigma^t\}$. (Note that we use subscripts to index variables and superscripts to index environments, such that σ_i^j denotes the i th intervention variable in environment j .) In each dataset, we measure a sample of post-treatment i.i.d. draws of some m -dimensional random vector X (possibly with $m \neq d$, as there is no reason to always assume a one-to-one mapping between intervention and random variables), and as an outcome Y . The data generating process $p(x; \sigma^j)$ is unknown. We assume $Y \perp\!\!\!\perp \sigma | X$, a conditional independence claim that can be tested with standard methods, and which holds automatically in cases where Y is a known deterministic summary of X . We are also given a factorization of $p(x; \sigma)$ that holds universally for all $\sigma \in \Sigma$,

$$p(x; \sigma) \propto \prod_{k=1}^l f_k(x_{S_k}; \sigma_{F_k}), \quad (1)$$

which we call an *interventional factor model* (IFM), where $S_k \subseteq [m]$ indexes a subset of the X variables and $F_k \subseteq [d]$ indexes a subset of the interventional variables (with each σ_i taking the value specified by the particular σ vector). The (positive) functions $f_k(\cdot; \cdot)$ are unknown. The model $p(y | x)$ can also be unknown, depending on the problem.

Scope and limitations. The factorization in Eq. (1) may come from different sources, e.g. from knowledge about physical connections (it is typically the case that one is able to postulate which variables are directly or only indirectly affected by an intervention) or as a result of structure learning methods (e.g., [1]). For structure learning, faithfulness-like assumptions [51] are required, as conditional independencies discovered under configurations Σ_{train} can only be extrapolated to Σ_{test} by assuming that independencies observed over particular values of σ can be generalized across all regimes. We do not commit to any particular structure learning technique, and refer to the literature on eliciting and learning graphical structure for a variety of methods [29].

The structural knowledge expressed by the factorization in Eq. (1) may be uninformative. Depending on the nature of Σ_{train} and Σ_{test} , it may be the case that we cannot generalize from training to test environments, and μ_{σ^*} is unidentifiable for all $\sigma^* \in \Sigma_{test}$, as we shall see in the sequel. However, all methods for causal inference rely on a trade-off between assumptions and informativeness. Unmeasured confounding may imply no independence constraints, for instance, but modeling unmeasured confounding is challenging, even more so for equilibrium data without observable dynamics. If we can get away with pure factorization constraints implied by an array of experimental conditions and domain knowledge, we should embrace this opportunity. This is what is done, for instance, in the literature on causal bandits and causal Bayesian optimization [31, 34, 3, 53], which leverage similar assumptions to decide what to do next. However, we are *not* proposing a method for bandits, Bayesian optimization or active learning. The task of estimating μ_{σ^*} for a novel regime is relevant in itself.

Factor graphs do not require a causal ordering, a concept which may be hard to justify in many applications and treated at length by e.g. [33]. While factor graph models do not enforce marginal independencies of the type $X_i \perp\!\!\!\perp \sigma_j$, which are characteristic of DAGs, our experiments in Section 5 suggest that approximated marginal independencies of this type can be easily learned.

3 Interventional Factor Model: Identification

We define our *identification problem* as follows: given the population distribution functions $\mathbb{P}(\Sigma_{train}) := \{p(x; \sigma^1), p(x; \sigma^2), \dots, p(x; \sigma^t)\}$ for regimes $\Sigma_{train} := \{\sigma^1, \sigma^2, \dots, \sigma^t\}$, and knowledge of the factorization assumptions as given by Eq. (1), can we identify a given $p(x; \sigma^*)$ corresponding to some σ^* regime in Σ_{test} ?

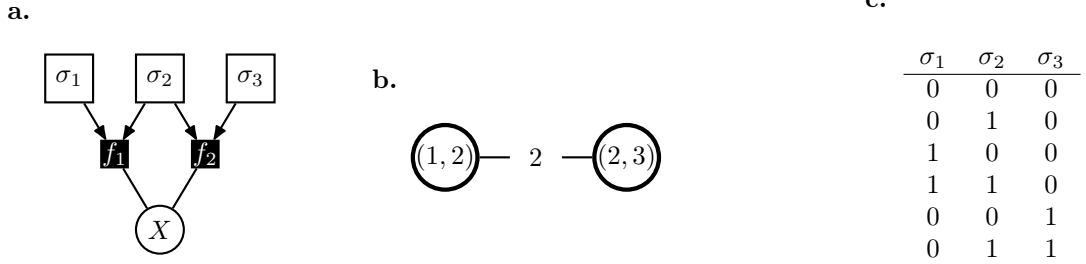


Figure 2: (a) An interventional factor graph with three intervention vertices. (b) Intervention vertices can be arranged as a *hypergraph* where hypervertex $(1, 2)$ represents set (σ_1, σ_2) and the edge represents the overlap between the two sets of intervention variables. In (c), a table showing the contents of a Σ_{train} set. From this set and the assumptions in (a), it is possible to infer what happens when $\sigma_1 = \sigma_2 = \sigma_3 = 1$ (also true for the other missing entry, $\sigma_1 = \sigma_3 = 1, \sigma_2 = 0$).

This identification problem is not analyzed in setups such as causal Bayesian optimization [3, 53], which model $p(x; \sigma)$ or μ_σ directly. Without this analysis, it is unclear to what extent much of the learning is an artefact of the choice of prior distribution or regularization, particularly for a sparsely populated Σ_{train} . As an extreme case that is not uncommon in practice, if we have binary intervention variables and we never observe more than one σ_i set to 1 within the same experiment, it is unclear why we should expect a non-linear model to provide information about pairs of assignments $\sigma_i = \sigma_j = 1$ using an off-the-shelf prior or regularizer. Although eventually a dense enough process of exploration will enrich the database of experiments, this process may be slow and less suitable to situations where the goal is not just to maximize some expected reward but to provide a more extensive picture of the dose-response relationships in a domain.

While the smoothness of $p(x; \sigma)$ as a function of σ is relevant domain-specific information, it complicates identifiability criteria without further assumptions. In what follows, we will assume no smoothness conditions, meaning that for some pair $p(x; \sigma^a), p(x; \sigma^b)$, where $a \neq b$, such probability density/mass functions are allowed to be arbitrarily different. This is particularly relevant when interventions take categorical levels with limited to no magnitude information.

Identification: preliminaries. Before introducing the main result of this section, let us start with a simple example from Fig. 2. The model in Fig. 2(a) shows a graph (how X could be factorized is not relevant here), and Fig. 2(c) shows a set Σ_{train} within a table. This set is lacking the experimental assignment $\sigma_1 = \sigma_2 = \sigma_3 = 1$.² However, this is implied by the graph and Σ_{train} . To see this, consider the implied factorization $p(x; \sigma) \propto f_1(x; \sigma_1, \sigma_2) f_2(x; \sigma_2, \sigma_3)$. This implies:

$$\frac{p(x; (1, 1, 0))}{p(x; (0, 1, 0))} \propto \frac{f_1(x; (1, 1))}{f_1(x; (0, 1))},$$

where we used $(1, 1, 0)$ etc. to represent assignments to σ that should be clear from context. Because both $(1, 1, 0)$ and $(0, 1, 0)$ are in Σ_{train} , the ratio is identifiable up to a multiplicative constant.

Moreover, multiplying and dividing the result by $f_2(x; (1, 1))$, we get:

$$\frac{p(x; (1, 1, 0))}{p(x; (0, 1, 0))} \propto \frac{f_1(x; (1, 1))}{f_1(x; (0, 1))} \frac{f_2(x; (1, 1))}{f_2(x; (1, 1))} \propto \frac{p(x; (1, 1, 1))}{p(x; (0, 1, 1))},$$

from which, given that $(0, 1, 1)$ is also in Σ_{train} , we can derive $p(x; (1, 1, 1))$.

3.1 Message Passing Formulation

The steps in this reasoning can be visualized in Fig. 2(b). There, the leftmost *hypervertex* represents (σ_1, σ_2) and suggests σ_1 can be isolated from σ_3 . The first ratio $p(x; (1, 1, 0))/p(x; (0, 1, 0))$ considers three roles: σ_1 can be isolated (it is set to a “baseline” of 0 in the denominator) and σ_3 is yet to be considered (it is set to the baseline value of 0 in the numerator). This ratio sets the stage for the next step where (σ_2, σ_3) is “absorbed” in the construction of the model evaluated at $(1, 1, 1)$. The entries in Σ_{train} were chosen so that we see all four combinations of (σ_1, σ_2) , and all four combinations of (σ_2, σ_3) , while avoiding the requirement for all eight combinations of $(\sigma_1, \sigma_2, \sigma_3)$. How to generalize this idea is the challenge. Next, we present our first proposed solution.

²As well as the assignment $\sigma_1 = \sigma_3 = 1, \sigma_2 = 0$, which can be recovered by an analogous argument.

Definitions. Before we proceed, we need a few definitions. First, we call the regime $\sigma_1 = \sigma_2 = \dots = \sigma_d = 0$ the *baseline* (or “observational”) regime. This describes data captured under a default protocol, e.g. a transcriptomic study in which no genes are knocked down.

Let $\Sigma_{[Z]}^0$ denote the set of all environments $\sigma^i \in \Sigma$ such that $\sigma_j^i = 0$ if $j \notin Z$. For instance, continuing the example in Fig. 1(b), a set $Z := \{2\}$ implies that $\Sigma_{[Z]}^0 = \{(0, 0, 0), (0, 1, 0)\}$. Finally, let $\sigma^{[Z^*(\star)]}$ be the intervention vector given by $\sigma_i = \sigma_i^*$, if $i \in Z$, and 0 otherwise.

An IFM \mathcal{I} with intervention vertices $\sigma_1, \dots, \sigma_d$ has an associated σ -graph denoted by $\mathcal{G}_{\sigma(\mathcal{I})}$, defined as an undirected graph with vertices $\sigma_1, \dots, \sigma_d$, and where edge $\sigma_i - \sigma_j$ is present if and only if σ_i and σ_j are simultaneously present in at least one common factor f_k in \mathcal{I} . In what follows, we make use of the concepts of graph *decompositions*, *decomposable graphs* and *junction trees*, as commonly applied to graphical models [32, 16]. For completeness, these concepts are reviewed in Appendix A. For instance, the σ -graph of the IFM represented in Fig. 2(a) is $\sigma_1 - \sigma_2 - \sigma_3$. This is a decomposable graph with vertex partition $A = \{\sigma_1\}$, $B = \{\sigma_2\}$ and $C = \{\sigma_3\}$. As this σ -graph is an undirected decomposable graph, it has a junction tree, which we depict in Fig. 2(b).

Identification: message passing formulation. Let \mathcal{I} be an IFM representing a collection of probabilistic models for a random vector X of dimension m indexed by an intervention vector σ of length d and domain Σ . Model \mathcal{I} has unknown factors but a known factorization $p(x; \sigma) \propto \prod_k f_k(x_{S_k}; \sigma_{F_k})$.

Theorem 3.1. *Assume that the σ -graph $\mathcal{G}_{\sigma(\mathcal{I})}$ is decomposable. Given a set $\Sigma_{train} = \{\sigma^1, \dots, \sigma^t\} \subseteq \Sigma$ and known distributions $p(x; \sigma^1), \dots, p(x; \sigma^t)$, the following conditions are sufficient to identify any $p(x; \sigma^*)$, $\sigma^* \in \Sigma$: i) all distributions indexed by $\sigma^1, \dots, \sigma^t, \sigma^*$ have the same support; and ii) $\Sigma_{[F_k]}^0 \in \Sigma_{train}$ for all F_k in the factorization of \mathcal{I} . The algorithm for computing $p(x; \sigma^*)$ works as follows. Construct a junction tree \mathcal{T} for \mathcal{I} , choose an arbitrary vertex in \mathcal{T} to be the root, and direct \mathcal{T} accordingly. If V_k is a hypervertex in \mathcal{T} , let D_k be the union of all intervention variables contained in the descendants of V_k in \mathcal{T} . Let B_k be the intersection of the intervention variables contained in V_k with the intervention variables contained in the parent $V_{\pi(k)}$ of V_k in \mathcal{T} .*

We define a message from a non-root vertex V_k to its parent $V_{\pi(k)}$ as

$$m_k^x := \frac{p(x; \sigma^{[D_k(\star)]})}{p(x; \sigma^{[B_k(\star)]})}, \quad (2)$$

with the update equation

$$p(x; \sigma^{[D_k(\star)]}) \propto p(x; \sigma^{[F_k(\star)]}) \prod_{V_{k'} \in ch(k)} m_{k'}^x, \quad (3)$$

where the product over $ch(k)$, the children of V_k in \mathcal{T} , is defined to be 1 if $ch(k) = \emptyset$. \square

(All proofs in Appendix A.) In particular, if no factor contains more than one intervention variable, the corresponding σ -graph will be fully disconnected. This happens, for example, for an IFM derived from a DAG without hidden variables and where each intervention has one child, as in Fig. 1.

3.2 Algebraic Formulation

If a σ -graph is not decomposable, the usual trick of triangulation prior to clique extraction can be used [32, 16], at the cost of creating cliques which are larger than the original factors. Alternatively, inspired by Eqs. (2) and (3), we consider transformations of the distributions in $\mathbb{P}(\Sigma_{train})$ by products and ratios. We define a *PR-transformation* of a density set $\{p(x; \sigma_1), \dots, p(x; \sigma_t)\}$ as any formula $\prod_{i=1}^t p(x; \sigma^i)^{q_i}$, for a collection q_1, \dots, q_t of real numbers.

Theorem 3.2. *Let $\sigma_{F_k}^v$ denote a particular value of σ_{F_k} , and let \mathbb{D}_k be the domain of σ_{F_k} . Given a collection $\mathbb{P}(\Sigma_{train}) := \{p(x; \sigma^1), \dots, p(x; \sigma^t)\}$ and a postulated model factorization $p(x; \sigma) \propto \prod_{k=1}^l f_k(x_{S_k}; \sigma_{F_k})$, a sufficient and almost-everywhere necessary condition for a given $p(x; \sigma^*)$ to be identifiable by PR-transformations of $\mathbb{P}(\Sigma_{train})$ is that there exists some solution to the system*

$$\forall k \in \{1, 2, \dots, l\}, \forall \sigma_{F_k}^v \in \mathbb{D}_k, \left(\sum_{i=1: \sigma_{F_k}^i = \sigma_{F_k}^v}^t q_i \right) = \mathbb{1}(\sigma_{F_k}^* = \sigma_{F_k}^v), \quad (4)$$

where $\mathbb{1}(\cdot)$ is the indicator function returning 1 or 0 if its argument is true or false, respectively. \square

	σ_1	σ_2	σ_3	f_1^{00}	f_1^{01}	f_1^{10}	f_1^{11}	f_2^{00}	f_2^{01}	f_2^{10}	f_2^{11}	f_3^{00}	f_3^{01}	f_3^{10}	f_3^{11}
q_1	0	0	0	✓				✓				✓			
q_2	0	1	0		✓					✓		✓			
q_3	1	0	0			✓		✓						✓	
q_4	1	1	0				✓			✓				✓	
q_5	0	0	1	✓					✓				✓		
q_6	0	1	1		✓						✓		✓		
q_7	1	0	1			✓			✓						✓
p^*	1	1	1	0	0	0	1	0	0	0	1	0	0	0	1

Figure 3: Example of how to infer the target distribution $p(x; (1, 1, 1))$ from the other seven possible regimes given the postulated factorization $p(x; \sigma) \propto f_1(x; \sigma_1, \sigma_2) f_2(x; \sigma_2, \sigma_3) f_3(x; \sigma_1, \sigma_3)$, the target distribution $p(x; (1, 1, 1))$. We used f_k^{ab} as a shorthand notation for $f_k(x; \sigma_{k_1} = a, \sigma_{k_2} = b)$, for σ_{k_1} and σ_{k_2} as given by context. For a PR-transformation $(f_1^{00} f_2^{00} f_3^{00})^{q_1} \times (f_1^{01} f_2^{10} f_3^{00})^{q_2} \times \dots \times (f_1^{10} f_2^{01} f_3^{11})^{q_7}$ to form an algebraic identity with $f_1^{11} f_2^{11} f_3^{11}$ up to a multiplicative constant independent of x , we need to find a solution satisfying $q_1 + q_5 = 0$, $q_2 + q_6 = 0$, \dots , $q_7 = 1$. A solution is $q_1 = q_4 = q_6 = q_7 = 1$, $q_2 = q_3 = q_5 = -1$, corresponding to $p(x; \sigma^*) \propto p(x; \sigma^1) p(x; \sigma^4) p(x; \sigma^6) p(x; \sigma^7) / \{p(x; \sigma^2) p(x; \sigma^3) p(x; \sigma^5)\}$.

An example of an application of this theorem is shown in Fig. 3. The solution to the system gives the PR-transformation. The message passing scheme and the algebraic method provide complementary views, with the former giving a divide-and-conquer perspective that identifies subsystems that can be estimated without requiring changes from the baseline treatment everywhere else. The algebraic method is more general, but suggests no hierarchy of simpler problems. These results show that the factorization over X is unimportant for identifiability, which may be surprising. We discuss the consequences of this finding to elicitation and testability in Appendix B.

4 Learning Algorithms

Theorems 3.1 and 3.2 provide ways of constructing a target distribution $p(x; \sigma^*)$ from products of ratios of densities from $\mathbb{P}(\Sigma_{train})$. However, in practice, we found that fitting a likelihood function directly often works better than estimating the product of density ratios, even for intractable likelihoods. We will discuss three strategies, all of which are demonstrated in the following section.

Deep energy-based models and direct regression. The most direct learning algorithm is to first maximize the sum of log-likelihoods $\mathcal{L}(\theta; \mathcal{D}^1, \dots, \mathcal{D}^l) := \sum_{i=1}^l \sum_{j=1}^{n_i} \log p_\theta(x^{ij}; \sigma^i)$, where x^{ij} is the j th sample from \mathcal{D}^i and n_i is the number of respective samples. The parameterization of the model is indexed by a vector θ , which defines $p(\cdot)$ as $\log p_\theta(x; \sigma) := \sum_{k=1}^l \phi_{\theta_{k, \sigma_{F_k}}}(x_{S_k}) + \text{constant}$. Here, $\phi_\theta(\cdot)$ is a differentiable black-box function, which in our experiments will be a multilayer perceptron (MLP). Parameter vector $\theta_{k, \sigma_{F_k}}$ is the collection of weights and biases of the MLP, a different instance for each factor k and combination of values in σ_{F_k} . In principle, making the parameters smooth functions of σ_{F_k} is possible, but in the interest of simplifying the presentation, we instead use a look-up table for completely independent parameters as indexed by the possible values of σ_{F_k} . Parameter set θ is the union of all $\sum_{k=1}^l \prod_{j \in F_k} |\mathcal{N}_j|$ MLP parameter sets. As maximizing log-likelihood is generally intractable, in our implementation we apply pseudo-likelihood with discretization of each variable X in a grid. The level of discretization does not affect the number of parameters, as we take their numerical value as is, renormalizing over the pre-defined grid. Score matching [27], noise contrastive estimation [24] or other variants (e.g., [50]) could be used; our pipeline is agnostic to this choice. We then estimate $f_y(x) := \mathbb{E}[Y | x]$ using an off-the-shelf method, which in our case is another MLP. For a given σ^* , we sample from the corresponding $p(x; \sigma^*)$ with Gibbs sampling and average the results of the regression estimate $\hat{f}_y(x)$ to obtain an estimate $\hat{\mu}_{\sigma^*}$.

Inverse probability weighting (IPW). A more direct method is to reweight each training sample by the target distribution $p(x; \sigma^*)$ to generate $\hat{\mu}_{\sigma^{*(i)}} := \sum_{j=1}^{n_i} y^{ij} w^{ij^*}$, where w^{ij^*} is the density ratio $p(x^{ij}; \sigma^*) / p(x^{ij}; \sigma^i)$, rescaled such that $\sum_{j=1}^{n_i} w^{ij^*} = 1$. There are several direct methods for density ratio estimation [38] that could be combined using the messages/product-ratios of the previous section, but we found that it was stabler to just take the density ratio of the fitted models using deep energy-based learning, just like in the previous algorithm. Once estimators $\hat{\mu}_{\sigma^{*(1)}}, \dots, \hat{\mu}_{\sigma^{*(l)}}$ are obtained, we combine

them by the usual inverse variance weighting rule, $\hat{\mu}_{\sigma^*} := \sum_{i=1}^t r^i \mu_{\sigma^*(i)} / \sum_{i=1}^t r^i$, where $r^i := 1/\hat{v}^i$, and $\hat{v}^i := \sum_{j=1}^{n_i} (y^{ij})^2 (w^{ij})^2$. The IPW method requires neither a model for $f_y(x)$ nor Markov chain Monte Carlo. However, it may behave more erratically than the direct method described above, particularly under strong shifts in distribution.

Covariate shift regression. Finally, a third approach for estimating μ_{σ^*} is to combine models for $f_y(x)$ with density ratios, learning a customized $\hat{f}_y(x)$ for each test regime separately. As this is very slow and did not appear to be advantageous compared to the direct method, we defer a more complete description to Appendix C.

Coverage. Even when treatment effects are identifiable within the IFM framework, the uncertainty of resulting estimates can vary widely depending on the training data and learning algorithm. Building on recent work in conformal inference [56, 36, 54], we derive the following finite sample coverage guarantee, which requires no extra assumptions beyond those stated above. We adapt the split conformal approach of [36] to the multi-regime setting by defining a *regime-wise even partition* as one that splits training data into two subsets on a stratified basis. That is, we construct subsets $\mathcal{I}_1, \mathcal{I}_2$ by putting half the samples from \mathcal{D}^1 into each, then doing the same for \mathcal{D}^2 , and so on through \mathcal{D}^t , thereby ensuring that regimes are equally represented in both subsets.

Theorem 4.1 (Coverage.). *Assume the identifiability conditions of Theorems 3.1 or 3.2 hold. Fix a target level $\alpha \in (0, 1)$ and let $\mathcal{I}_1, \mathcal{I}_2$ be a regime-wise even partition of the n training samples. Fit a model $\hat{f}_y(x)$ using only data from \mathcal{I}_1 . Compute conformity scores $s(x, y) = |y - \hat{f}_y(x)|$ using only data from \mathcal{I}_2 . Define the normalized likelihood ratio $w(x, \sigma^*) \propto p(x; \sigma^*)/p(x; \sigma)$, rescaled to sum to unity over samples in \mathcal{I}_2 . Define the weighted conformity score $\tilde{s}_{\sigma^*}(x, y) := s(x, y) \cdot w(x, \sigma^*)$. Let τ_{σ^*} be the q^{th} smallest value in $\tilde{s}_{\sigma^*}(x, y)$, with $q = \lceil (n/2 + 1)(1 - \alpha) \rceil$. Then we have:*

$$\mathbb{P}(\mu_{\sigma^*} \in \hat{\mu}_{\sigma^*} \pm \tau_{\sigma^*}) \geq 1 - \alpha.$$

Moreover, if weighted conformity scores have a continuous joint distribution, then the upper bound on this probability is $1 - \alpha + 2/(n + 2)$. \square

5 Experiments

We run a number of semi-synthetic experiments to evaluate the performance of the IFM approach on a range of intervention generalization tasks. Full details on datasets and model hyperparameters can be found in Appendix D. Code for reproducing all results and figures is available online.³

Our experiments are based on the following biomolecular datasets (see Appendix D.1 for details): i) **Sachs** [45]: This dataset comes from a cellular signaling network with 11 nodes representing phosphorylated proteins and phospholipids, several of which were perturbed with targeted reagents to stimulate or inhibit expression. All intervention variables are binary. We train on 5 data regimes (*baseline*, with all $\sigma_i = 0$, and all four regimes with a single $\sigma_i = 1$). Σ_{test} is defined on the remaining 11 ($= 2^4 - 5$) unseen regimes. ii) **DREAM** [22]: The Dialogue for Reverse Engineering Assessments and Methods (DREAM) challenge spans a set of regulatory network inference benchmarks. We generate data based on a known *E. coli* sub-network with 10 nodes using GeneNetWeaver [47]. All interventions are binary, and again Σ_{train} is defined by baseline $\sigma = 0$ and the 10 single choices of $\sigma_i = 1$. Σ_{test} consists of 45 ($10 \times 9/2 = 45$) unseen regimes defined by all pairs $\sigma_i = \sigma_j = 1$.

We compare IFM to the following benchmarks: i) **Black-box**: We apply an off-the-shelf algorithm (in this case, XGBoost [11]) to learn a direct mapping from σ to Y without using any information on X . Compared with our proposed model, the black-box model does not exploit any structural assumptions. ii) **DAG**: We estimate the structural equations in an acyclic topological ordering that is consistent with the data generating process. This represents a strong baseline that exploits structural assumptions. The likelihood is defined by conditional Gaussian models with mean and variances parameterized as MLPs, matching exactly one of the simulators described below. We implement three variants of our proposed IFM model, corresponding to the three learning algorithms described in Section 4: i) **IFM1** uses deep energy-based models and direct regression; ii) **IFM2** uses an IPW estimator; and iii) **IFM3** relies on covariate shift regression. See Appendix D.4 for more details.

³<https://github.com/rbas-ucl/intgen>.

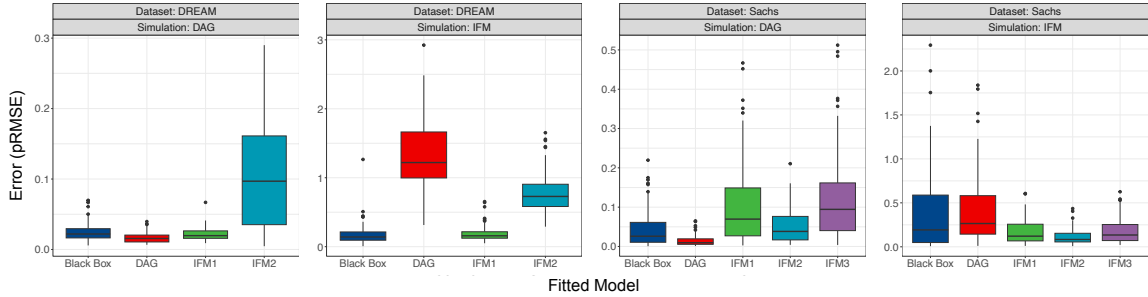


Figure 4: Experimental results on a range of intervention generalization tasks, see text for details.

Oracular Simulators. The first step to test intervention generalization is to build a set of proper test beds (i.e., simulators that serve as causal effect oracles for any $\sigma \in \Sigma$), motivated by expert knowledge about the underlying system dynamics. Neither the original Sachs data nor the DREAM simulator we used provide joint intervention data required in our evaluation.

Hence, for each domain, we train two *ground truth simulators*: i) *Causal-DAG*, a DAG model following the DAG structure and data provided by the original Sachs et al. and DREAM sources. The graphs, including respective intervention vertices, are described in Appendix D.1. Given the DAG, we fit a model where each conditional distribution is heteroskedastic Gaussian with mean and variance parameterized by MLP functions (each with 10 hidden units) of the respective parents; ii) *Causal-IFM*, where the graph is a direct projection of the postulated DAG factors by moralization and direction dropping [32, as in e.g. Fig. 1(b)]. The likelihood is a neural energy model (Section 4) with MLPs of 15 hidden units defining potential functions. After fitting these two models, we compute by Monte Carlo simulation their implied ground truths for every choice of σ^* in the respective Σ_{test} , using synthetic models $p(y | x)$ defined below. These simulators also provide training data for all subsequent experiments. See Appendix D.2 for more details.

To generate training datasets of the general form (σ, x, y) for each σ , we simulate 5000 samples from the baseline regime and 500 from each remaining regime (4 for Sachs and 10 for DREAM). Causal effects Y are generated under 100 different structural equations of the form $\tanh(\lambda^\top X) + \epsilon$, with random independent normal weights λ and $\epsilon \sim \mathcal{N}(0, v_y)$. λ and v_y are scaled such that the ground truth variance of $\lambda^\top X$ is a number v_x sampled uniformly at random from the interval $[0.6, 0.8]$, and set $v_y := 1 - v_x$. See Appendix D.3 for more details.

Results. We evaluate model performance based on the proportional root mean squared error (pRMSE), defined as the average of the squared difference between the ground truth Y and estimated \hat{Y} , with each entry further divided by the ground truth variance of the corresponding Y . Results are visualized in Fig. 4. We additionally run a series of one-sided binomial tests to determine whether models significantly outperform the black box baseline, and compare the Spearman rank correlation between expected and observed outcomes for all test regimes (see Appendix E.2.)

Unsurprisingly, DAGs do best when the ground truth is a Causal-DAG, while IFM methods fare better when the data generator is a Causal-IFM. Among the three variants of IFM models, the IPW methods underperform on DREAM datasets, which may be because the knockdowns regimes in those datasets induce dramatic shifts in distribution overlap among regimes. However, IFMs are notably robust to simulation settings, with IFM1 (the deep energy model) doing especially well on the DREAM dataset, and IFM2 (the IPW estimator) excelling on the Sachs data. (We omit results for IFM3 (covariate shift regression) on the DREAM dataset, as the method does not converge in a reasonable time.) Though the black box model sometimes struggles to extrapolate with a long-tail of errors, XGBoost actually does surprisingly well in some experiments, especially on the DREAM dataset. It must be pointed out that the black-box method is essentially indistinguishable from linear regression in this benchmark (results not shown), which is not surprising given how sparse the training data is. However, the non-additivity of the σ effect on Y is more prominent in the Sachs data, making it difficult to generalize without structural assumptions. Together, these results illustrate the promise of IFMs for interventional generalization problems (see Appendix E for more results and analysis).

6 Related Work

Several authors exploit structural assumptions to predict the effects of unseen treatments. Much of this research falls under the framework of *transportability* [42, 5], where the goal is to identify causal estimands from a combination of observational and/or experimental data collected under different regimes. Pearl’s *do*-calculus is known to be sound and complete for this task under atomic interventions [35], while the σ -calculus, originally introduced by [20, 14], extends transportability results to so-called “soft” interventions [13, 15]. These methods generally assume that the data generating distribution is represented by an underlying DAG. DAG models with additive errors have some identifiability [46] and estimation [53] advantages, but acyclic error additivity may not be a believable assumption in some domains. Under further parametric assumptions, causal effects can be imputed with matrix completion techniques [2, 52, 2] or more generic supervised learning approaches [23], but they require some data to be collected for all regimes in Σ_{test} .

Another strand of related research pertains to online learning contexts. For instance, several authors have shown that causal information can boost convergence rates in multi-armed bandit problems when dependencies are present between arms [31, 34, 18], even when these structures must themselves be adaptively learned [7]. These represent a promising direction for future work, where identification strategies based on the IFM framework are used to prioritize the search for optimal treatments. Pooling samples across multiple regimes can be an effective strategy for causal discovery, as illustrated by recent advances in invariant causal prediction [43, 25, 44, 57]. It can also help with domain adaptation and covariate shift, where the goal is to stabilize performance under various perturbations to the data generating process [39, 4, 10, 12].

7 Conclusion

We introduced the IFM framework for solving intervention generalization tasks. Results from simulations calibrated by real-world data show that our method successfully predicts outcomes for novel treatments, providing practitioners with new methods for conducting synthetic experiments. Future work includes: i) integrating the approach with experimental design, Bayesian optimization and bandit learning; ii) variations that include pre-treatment variables and generalizations across heterogeneous subpopulations, inspired by complementary matrix factorization methods such as [2]; iii) tackling sequential treatments; and iv) diagnostics of cross-regime overlap issues [26, 40].

Acknowledgments

This work was partially supported by ONR grant 62909-19-1-2096 and EPSRC fellowship EP/W024330/1. JZ was supported by UKRI grant EP/S021566/1.

References

- [1] P. Abbeel, D. Koller, and A. Y. Ng. Learning factor graphs in polynomial time and sample complexity. *Journal of Machine Learning Research*, 7:1743–1788, 2006.
- [2] Abhineet Agarwal, Anish Agarwal, and Suhas Vijaykumar. Synthetic combinations: A causal inference framework for combinatorial interventions. *arXiv preprint*, 2303.14226, 2023.
- [3] V. Aglietti, X. Lu, A. Paleyes, and J. González. Causal Bayesian optimization. *23rd International Conference on Artificial Intelligence and Statistics*, 2020.
- [4] Martin Arjovsky, Léon Bottou, Ishaan Gulrajani, and David Lopez-Paz. Invariant risk minimization. *arXiv preprint*, 1907.02893, 2020.
- [5] Elias Bareinboim and Judea Pearl. Transportability from multiple environments with limited experiments: Completeness results. In *Advances in Neural Information Processing Systems*, volume 27, 2014.
- [6] Ioana Bica, Ahmed M. Alaa, Craig Lambert, and Mihaela van der Schaar. From real-world patient data to individualized treatment effects using machine learning: Current and future methods to address underlying challenges. *Clinical Pharmacology & Therapeutics*, 109(1):87–100, 2021.
- [7] Blair Bilodeau, Linbo Wang, and Daniel M. Roy. Adaptively exploiting d -separators with causal bandits. In *Advances in Neural Information Processing Systems*, 2022.

- [8] T. Blom and J. M. Mooij. Causality and independence in perfectly adapted dynamical systems. *Journal of Causal Inference*, 11(1):2885–2915, 2023.
- [9] S. Bongers, Pa. Forré, J. Peters, and J. M. Mooij. Foundations of structural causal models with cycles and latent variables. *Annals of Statistics*, 49(5):2885–2915, 2021.
- [10] Peter Bühlmann. Invariance, Causality and Robustness. *Statistical Science*, 35(3):404 – 426, 2020.
- [11] Tianqi Chen and Carlos Guestrin. XGBoost: A scalable tree boosting system. In *Proceedings of the 22nd ACM SIGKDD International Conference on Knowledge Discovery and Data Mining*, page 785–794, 2016.
- [12] Yuansi Chen and Peter Bühlmann. Domain adaptation under structural causal models. *J. Mach. Learn. Res.*, 22(1), 2021.
- [13] Juan Correa and Elias Bareinboim. General transportability of soft interventions: Completeness results. In *Advances in Neural Information Processing Systems*, volume 33, pages 10902–10912, 2020.
- [14] Juan Correa and Elias Bareinboim. A calculus for stochastic interventions: causal effect identification and surrogate experiments. *Proceedings of the AAAI Conference on Artificial Intelligence*, 34(06):10093–10100, 2020.
- [15] Juan Correa, Sanghack Lee, and Elias Bareinboim. Counterfactual transportability: A formal approach. In *International Conference on Machine Learning*, 2022.
- [16] R. Cowell, A. Dawid, S. Lauritzen, and D. Spiegelhalter. *Probabilistic Networks and Expert Systems*. Springer-Verlag, 1999.
- [17] P. Dawid. Decision-theoretic foundations for statistical causality. *Journal of Causal Inference*, 9(56):39–77, 2021.
- [18] Arnoud A. W. M. de Kroon, Danielle Belgrave, and Joris M. Mooij. Causal discovery for causal bandits utilizing separating sets. *arXiv:2009.07916*, 2020.
- [19] M. Drton. Discrete chain graph models. *Bernoulli*, 15:736–753, 2009.
- [20] Patrick Forré and Joris M Mooij. Constraint-based causal discovery for non-linear structural causal models with cycles and latent confounders. In *Proceedings of the 34th Annual Conference on Uncertainty in Artificial Intelligence*, pages 269–278, 2018.
- [21] Amanda M Gentzel, Purva Pruthi, and David Jensen. How and why to use experimental data to evaluate methods for observational causal inference. In *International Conference on Machine Learning*, pages 3660–3671. PMLR, 2021.
- [22] Alex Greenfield, Aviv Madar, Harry Ostrer, and Richard Bonneau. Dream4: Combining genetic and dynamic information to identify biological networks and dynamical models. *PloS one*, 5(10):e13397, 2010.
- [23] Limor Gultchin, David Watson, Matt Kusner, and Ricardo Silva. Operationalizing complex causes: A pragmatic view of mediation. In *Proceedings of the 38th International Conference on Machine Learning*, volume 139 of *Proceedings of Machine Learning Research*, pages 3875–3885. PMLR, 2021.
- [24] M. Gutmann and A. Hyvärinen. Noise-contrastive estimation: A new estimation principle for unnormalized statistical models. *13th International Conference on Artificial Intelligence and Statistics (AISTATS)*, pages 297–304, 2010.
- [25] Christina Heinze-Deml, Jonas Peters, and Nicolai Meinshausen. Invariant Causal Prediction for Nonlinear Models. *J. Causal Inference*, 6(2), 2018.
- [26] J. Hill and Y.S. Su. Assessing lack of common support in causal inference using bayesian nonparametrics: Implications for evaluating the effect of breastfeeding on children’s cognitive outcomes. *The Annals of Applied Statistics*, 7:1386–1420, 2011.
- [27] A. Hyvärinen. Estimation of non-normalized statistical models by score matching. *Journal of Machine Learning Research*, 6:695–709, 2005.
- [28] Guy Karlebach and Ron Shamir. Modelling and analysis of gene regulatory networks. *Nature Reviews Molecular Cell Biology*, 9(10):770–780, 2008.
- [29] D. Koller and N. Friedman. *Probabilistic Graphical Models: Principles and Techniques*. MIT Press, 2009.

- [30] F. Kschischang, B. Frey, J. Brendan, and H-A. Loeliger. Factor graphs and the sum-product algorithm. *IEEE Transactions on Information Theory*, 47:498–519, 2001.
- [31] Finnian Lattimore, Tor Lattimore, and Mark D. Reid. Causal bandits: Learning good interventions via causal inference. In *Advances in Neural Information Processing Systems*, pages 1181–1189, 2016.
- [32] S. Lauritzen. *Graphical Models*. Oxford University Press, 1996.
- [33] S. L. Lauritzen and T. S. Richardson. Chain graph models and their causal interpretation. *Journal of the Royal Statistical Society Series B*, 64:321–361, 2002.
- [34] Sanghack Lee and Elias Bareinboim. Structural causal bandits: Where to intervene? In *Advances in Neural Information Processing Systems*, pages 2568–2578, 2018.
- [35] Sanghack Lee, Juan Correa, and Elias Bareinboim. General transportability – synthesizing observations and experiments from heterogeneous domains. *Proceedings of the AAAI Conference on Artificial Intelligence*, 34(06):10210–10217, 2020.
- [36] Jing Lei, Max G’Sell, Alessandro Rinaldo, Ryan J Tibshirani, and Larry Wasserman. Distribution-Free Predictive Inference for Regression. *Journal of the American Statistical Association*, 113(523):1094–1111, jul 2018.
- [37] Anja K Leist, Matthias Klee, Jung Hyun Kim, David H Rehkopf, Stéphane PA Bordas, Graciela Muniz-Terrera, and Sara Wade. Mapping of machine learning approaches for description, prediction, and causal inference in the social and health sciences. *Science Advances*, 8(42):eabk1942, 2022.
- [38] Nan Lu, Tianyi Zhang, Tongtong Fang, Takeshi Teshima, and Masashi Sugiyama. Rethinking importance weighting for transfer learning. In *Federated and Transfer Learning*, pages 185–231. Springer, 2023.
- [39] Sara Magliacane, Thijs van Ommen, Tom Claassen, Stephan Bongers, Philip Versteeg, and Joris M Mooij. Domain adaptation by using causal inference to predict invariant conditional distributions. In *Advances in Neural Information Processing Systems*, volume 31, 2018.
- [40] M. Oberst, F. Johansson, D. Wei, T. Gao, G. Brat, D. Sontaga, and K. Varshney. Characterization of overlap in observational studies. *23rd International Conference on Artificial Intelligence and Statistics (AISTATS 2020)*, pages 788–798, 2020.
- [41] J. Pearl. *Causality: Models, Reasoning and Inference, 2nd edition*. Cambridge University Press, 2009.
- [42] Judea Pearl and Elias Bareinboim. Transportability of causal and statistical relations: A formal approach. *Proceedings of the AAAI Conference on Artificial Intelligence*, 25(1):247–254, 2011.
- [43] Jonas Peters, Peter Bühlmann, and Nicolai Meinshausen. Causal inference by using invariant prediction: identification and confidence intervals. *J. Royal Stat. Soc. Ser. B Methodol.*, 78(5):947–1012, 2016.
- [44] Niklas Pfister, Peter Bühlmann, and Jonas Peters. Invariant causal prediction for sequential data. *Journal of the American Statistical Association*, 114(527):1264–1276, 2019.
- [45] K. Sachs, O. Perez, D. Pe’er, D. Lauffenburger, and G. Nolan. Causal protein-signaling networks derived from multiparameter single-cell data. *Science*, 308, 2005.
- [46] S. Saengkyongam and R. Silva. Learning joint nonlinear effects from single-variable interventions in the presence of hidden confounders. *36th Conference on Uncertainty in Artificial Intelligence (UAI 2020)*, 2020.
- [47] Thomas Schaffter, Daniel Marbach, and Dario Floreano. Genenetweaver: in silico benchmark generation and performance profiling of network inference methods. *Bioinformatics*, 27(16):2263–2270, 2011.
- [48] D. Sejdinovic, A. Gretton, and W. Bergsma. A kernel test for three-variable interactions. *Neural Information Processing Systems (NeurIPS)*, 26:1124–1132, 2013.
- [49] Claudia Shi, Dhanya Sridhar, Vishal Misra, and David Blei. On the assumptions of synthetic control methods. In *International Conference on Artificial Intelligence and Statistics*, pages 7163–7175. PMLR, 2022.
- [50] Y. Song and S. Ermon. Generative modeling by estimating gradients of the data distribution. *Neural Information Processing Systems (NeurIPS)*, 32, 2019.
- [51] P. Spirtes, C. Glymour, and R. Scheines. *Causation, Prediction and Search*. Cambridge University Press, 2000.

- [52] Chandler Squires, Dennis Shen, Anish Agarwal, Devavrat Shah, and Caroline Uhler. Causal imputation via synthetic interventions. In *Conference on Causal Learning and Reasoning*, pages 688–711. PMLR, 2022.
- [53] S. Sussex, A. Makarova, and A. Krause. Model-based causal Bayesian optimization. *11th International Conference on Learning Representations*, 2023.
- [54] Ryan J Tibshirani, Rina Foygel Barber, Emmanuel Candes, and Aaditya Ramdas. Conformal prediction under covariate shift. In *Advances in Neural Information Processing Systems*, volume 32, 2019.
- [55] Panagiotis Tigas, Yashas Annadani, Andrew Jesson, Bernhard Schölkopf, Yarin Gal, and Stefan Bauer. Interventions, where and how? Experimental design for causal models at scale. In *Neural Information Processing Systems (NeurIPS 2022)*, 2022.
- [56] Vladimir Vovk, Alexander Gammerman, and Glenn Shafer. *Algorithmic Learning in a Random World*. Springer, New York, 2005.
- [57] Amy Zhang, Clare Lyle, Shagun Sodhani, Angelos Filos, Marta Kwiatkowska, Joelle Pineau, Yarin Gal, and Doina Precup. Invariant causal prediction for block MDPs. In *Proceedings of the 37th International Conference on Machine Learning*, volume 119, pages 11214–11224. PMLR, 2020.

A Proofs of Identifiability and Further Examples

This section presents results concerning Theorems 3.1 and 3.2. We start with some background with textbook definitions, followed by proofs and examples for the decomposable graph, concluding with proofs for the purely algebraic case. The decomposable case sheds light on how to hierarchically structure products and ratios of $\mathbb{P}(\Sigma_{train})$. Among other uses, this theoretically suggests which regimes could be directly sampled from and added to Σ_{train} , in order to reduce the estimation error coming from particular product/ratios which are required to identify larger marginal distributions.

Background. A *decomposition* of an undirected graph \mathcal{G} is formed from a partition of its vertices into a triplet (A, B, C) where C is complete (a clique) and separates A from B . The decomposition is *proper* if both A and B are non-empty. Moreover, an undirected graph is *decomposable* if it is complete or, failing that, it has a proper decomposition into a triplet (A, B, C) , where the subgraph of \mathcal{G} with vertices $A \cup B$ and the subgraph with vertices $B \cup C$ are both decomposable.

A *junction tree* \mathcal{T} of a decomposable graph \mathcal{G} is a tree where each vertex V_i is labeled with the elements of a unique maximal clique from \mathcal{G} (hence, this type of vertex is sometimes called a *hypervertex*), so that $V_i \cap V_j$ denotes the corresponding intersection among sets of vertices in \mathcal{G} . Edges $V_i - V_j$ of \mathcal{T} are graphically represented with labels denoting the intersection $V_i \cap V_j$. A junction tree must have a *running intersection* property: any intersection $V_i \cap V_j$ must be contained in all vertices in the (unique) path between V_i and V_j in \mathcal{T} .

If $\mathcal{G}_{\sigma(\mathcal{I})}$ is decomposable, there exists at least one junction tree compatible with it. Let \mathcal{T} be one of them. Without loss of generality, pick an arbitrary vertex of \mathcal{T} to be the root and direct edges away from it to create a directed tree out of the junction tree, so that we can assume \mathcal{T} to be directed. We will prove identifiability by an induction argument that starts at the leaves of the directed junction tree, moving towards the (unique) parent of any particular vertex child in the induction step.

Definitions and notation. In what follows, we use V_k to denote a vertex in \mathcal{T} . By abuse of notation, depending on context, V_k is also used to denote the corresponding intervention variables σ_{F_k} in the original factor graph.

Let $\sigma^{[Z(w)]}$ be a particular instantiation of σ where $Z \subseteq [d]$ and $\sigma_Z = w$ (possibly a vector), with the remaining entries of σ being zero. For instance, if $d = 3$, $Z = \{2, 3\}$, and $w = (2, 1)$, then $\sigma^{[Z(w)]} = (0, 2, 1)$. Vector w is allowed to include zero values. To avoid subsequently heavy notation, from this point on we will use $\sigma^{[Z(*)]}$ to denote $\sigma^{[Z(\sigma_Z^*)]}$, that is, the vector of assignments that we obtain by setting to zero all entries of σ^* which are not in Z .

We use $ch(k)$ to denote the set of children of vertex V_k in \mathcal{T} , and $V_{\pi(k)}$ to denote its (unique) parent, if V_k is not the root vertex. Also, let D_k denote the union of the intervention variables contained in at least one descendant of V_k in \mathcal{T} , remembering that by convention V_k is also a descendant of itself. Finally, let $B_k := D_k \cap V_{\pi(k)}$, the set of intervention variables common to both D_k and $V_{\pi(k)}$. This means that, by the running intersection property of junction trees, B_k separates $A_k := D_k \setminus B_k$ from the rest of σ in the σ -graph $\mathcal{G}_{\sigma(\mathcal{I})}$.

Proof of Theorem 3.1. To simplify the proof, assume without loss of generality that no entry in σ^* is zero. To see this, if $\sigma_i^* = 0$, consider the factors k containing σ_i as being constants in σ_i , with scope S_k being redefined as $S_{k'} := S_k \setminus \{\sigma_i\}$. Σ_{train} in this redefined space still satisfies the assumption of having entries spanning all possible values for $\sigma_{S_{k'}}$ while holding the remaining intervention variables at the background level of 0. Likewise, as identifiability will be shown pointwise for a given σ^* (where the categorical labels for the intervention values are arbitrary symbols), we can assume all entries σ_i^* as being equal, and equal to 1.

We define a *message* from vertex V_k to its parent $V_{\pi(k)}$ as

$$m_k^x := \frac{p(x; \sigma^{[D_k(*)]})}{p(x; \sigma^{[B_k(*)]})}, \quad (5)$$

and state that

$$p(x; \sigma^{[D_k(*)]}) \propto p(x; \sigma^{[F_k(*)]}) \prod_{V_{k'} \in ch(k)} m_{k'}^x, \quad (6)$$

with the product over $ch(k)$ defined to be 1 if $ch(k) = \emptyset$. We will show how (5) can be recursively identified from a message scheduling that starts from the leaves and propagates messages towards the root of \mathcal{T} . We will show as well how Eq. (6) holds.

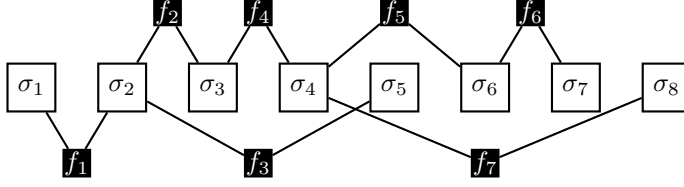


Figure 5: The factor graph used as an illustration of the technique in the proof of Theorem 3.1.

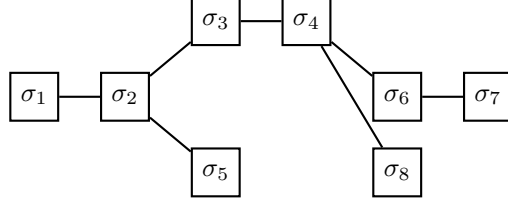


Figure 6: The σ -graph corresponding to the factor graph in Figure 5.

Let V_k be a leaf of \mathcal{T} . Then $D_k = F_k$ and $p(x; \sigma^{[F_k(\star)]})$ is identified as it is part of Σ_{train} , showing that Eq. (6) holds for the leaf vertices of \mathcal{T} . Likewise, message m_k^x is identifiable for leaf vertices, as both D_k and B_k are contained in F_k .

Let V_k now be an internal vertex of \mathcal{T} , and assume that Equations (5) and (6) are identified for all of its proper descendants. As all entries of σ^* are assumed to be 1, it will be useful to define $g_k := f_k(x; \sigma_{F_k} = 1)$. Also define $h_k := f_k(x; \sigma_{F_k \cap B_k} = 1, \sigma_{F_k \setminus B_k} = 0)$ and $z_k := f_k(x; \sigma_{F_k} = 0)$.

Since \mathcal{T} is a junction tree, D_k can be partitioned into sets $D_{k'}$, where $V_{k'} \in ch(k)$, or otherwise there would be a violation of the running intersection property. Let $Q(k')$ be the set of all indices of factors q where $F_q \subseteq D_{k'}$. Let

$$Q_{k'} := \prod_{q \in Q(k')} \frac{g_q}{h_q}.$$

We can multiply and divide $Q_{k'}$ by the product of all factors z_q where $F_q \cap D_{k'} = \emptyset$. This implies

$$Q_{k'} \propto \frac{p(x; \sigma^{[D_{k'}(\star)]})}{p(x; \sigma^{[B_{k'}(\star)]})} = m_{k'}^x.$$

Moreover, the product

$$\frac{\prod_{q: F_q \cap D_k = \emptyset} z_q}{\prod_{q: F_q \cap D_k = \emptyset} z_q} \times \frac{f_k(x; \sigma_{F_k} = 1)}{f_k(x; \sigma_{F_k} = 1)} \times \frac{f_{\pi(k)}(x; \sigma_{B_k} = 1, \sigma_{F_{\pi(k)} \setminus B_k} = 0)}{f_{\pi(k)}(x; \sigma_{B_k} = 1, \sigma_{F_{\pi(k)} \setminus B_k} = 0)} \times \prod_{k': V_{k'} \in ch(k)} Q_{k'}$$

is such that the numerator is proportional to $p(x; \sigma^{[D_k(\star)]})$ and the denominator is proportional to $p(x; \sigma^{[F_k(\star)]})$. To see this, notice that the numerator sets the σ_{F_j} variables for all factors F_j in a coherent way such that entries in D_k are set to 1 while everything else is set to zero (entries in D_k may still appear in $V_{\pi(k)}$, as $D_k \cap F_{\pi(k)} = B_k$, is possibly non-empty. Hence, we set to 1 those entries in $F_{\pi(k)}$ which are in B_k , explaining the appearance of the $f_{\pi(k)}$ factors in the expression above).

This implies

$$\frac{p(x; \sigma^{[D_k(\star)]})}{p(x; \sigma^{[F_k(\star)]})} \propto \prod_{V_{k'} \in ch(k)} m_{k'}^x,$$

from which Eq. (6) follows from quantities previously identified, and as such it identifies $p(x; \sigma^{[D_k(\star)]})$. To build message m_k^x , all that remains is $p(x; \sigma^{[B_k(\star)]})$. However, $B_k \subseteq F_k$, and since Σ_{train} contains the distribution $p(x; \sigma^{[H_k(\star)]})$ for all $H_k \subseteq F_k$, this is also identified. The required identifiability of $p(x; \sigma^*)$ follows from propagating these messages all the way up to the root of \mathcal{T} . \square

Example. Let's solve the example shown in Figures 5-7. The IFM itself is given by

$$p(x; \sigma) \propto f_1(x; \sigma_1, \sigma_2) f_2(x; \sigma_2, \sigma_3) f_3(x; \sigma_2, \sigma_5) f_4(x; \sigma_3, \sigma_4) f_5(x; \sigma_4, \sigma_6) f_6(x; \sigma_6, \sigma_7) f_7(x; \sigma_4, \sigma_8),$$

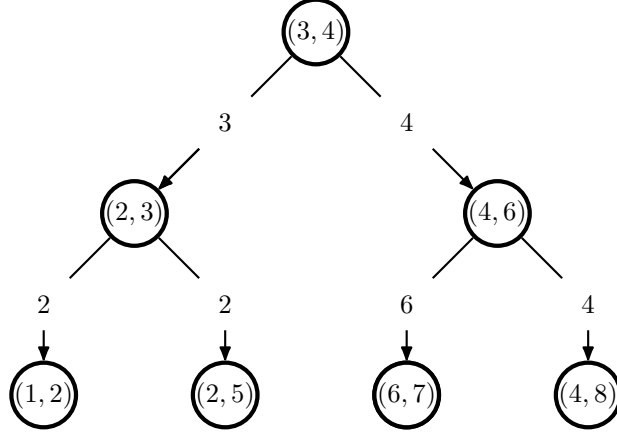


Figure 7: A (directed) junction tree corresponding to the undirected graph in Figure 6.

where all intervention variables are binary and we will generate the regime at $\sigma_1 = \sigma_2 = \dots = \sigma_8 = 1$. For reference, this means considering the following sets implied by the factorization above:

$$\begin{array}{lll}
F_1 = \{1, 2\} & D_1 = \{1, 2\} & B_1 = \{2\} \\
F_2 = \{2, 3\} & D_2 = \{1, 2, 3, 5\} & B_2 = \{3\} \\
F_3 = \{2, 5\} & D_3 = \{2, 5\} & B_3 = \{2\} \\
F_4 = \{3, 4\} & D_4 = \{1, 2, 3, 4, 5, 6, 7, 8\} & B_4 = \emptyset \\
F_5 = \{4, 6\} & D_5 = \{4, 6, 7, 8\} & B_5 = \{4\} \\
F_6 = \{6, 7\} & D_6 = \{6, 7\} & B_6 = \{6\} \\
F_7 = \{4, 8\} & D_7 = \{4, 8\} & B_7 = \{4\}
\end{array}$$

To illustrate how message passing will work, let's introduce some symbols so that the steps are easier to follow. Let g_{ij}^{11} represent a factor with $\sigma_i = \sigma_j = 1$. For instance, $g_{12}^{11} = f_1(x; \sigma_1 = 1, \sigma_2 = 1)$. This is slightly redundant compared to the notion in the proof (which uses " g_1 " to denote $f_1(x; \sigma_1 = 1, \sigma_2 = 1)$), but the redundancy of the superscripts will hopefully make it easier to visualize the logic in the steps that follow.

Likewise, let h_{ij}^{01} and h_{ij}^{10} denote assignments $(\sigma_i, \sigma_j) = (0, 1)$ and $(\sigma_i, \sigma_j) = (1, 0)$, respectively. Finally, let z_{ij}^{00} denote the respective factor with assignment $\sigma_i = \sigma_j = 0$.

We will use expressions such as $p(x; [ij])$ to denote $p(x; \sigma_i = 1, \sigma_j = 1, \sigma_{1:8 \setminus \{i,j\}} = 0)$ to make the notation simpler.

The messages at the leaves are

$$\begin{array}{ll}
m_1^x & = p(x; [12])/p(x; [2]) \quad (D_1 = \{1, 2\}, B_1 = \{2\}) \\
m_3^x & = p(x; [25])/p(x; [2]) \quad (D_3 = \{2, 5\}, B_3 = \{2\}) \\
m_6^x & = p(x; [67])/p(x; [6]) \quad (D_6 = \{6, 7\}, B_6 = \{6\}) \\
m_7^x & = p(x; [48])/p(x; [4]) \quad (D_7 = \{4, 8\}, B_7 = \{4\})
\end{array}$$

It can be readily verified that all of these are identifiable from Σ_{train} , as all non-zero assignments are contained within some factor.

Now, let's pass messages to (2, 3) using formula (6). To see how it is applicable, start from

$$\begin{aligned}
m_1^x \times m_3^x &= \frac{p(x; [12])}{p(x; [2])} \frac{p(x; [25])}{p(x; [2])} \\
&\propto \frac{g_{12}^{11} h_{23}^{10} h_{25}^{10} z_{34}^{00} z_{46}^{00} z_{67}^{00} z_{48}^{00}}{h_{12}^{01} h_{23}^{10} h_{25}^{10} z_{34}^{00} z_{46}^{00} z_{67}^{00} z_{48}^{00}} \times \frac{h_{12}^{01} h_{23}^{10} g_{25}^{11} z_{34}^{00} z_{46}^{00} z_{67}^{00} z_{48}^{00}}{h_{12}^{01} h_{23}^{10} h_{25}^{10} z_{34}^{00} z_{46}^{00} z_{67}^{00} z_{48}^{00}}
\end{aligned}$$

Now, we multiply and divide it by the factor of (2, 3) and its parent (3, 4) evaluated at $(\sigma_2, \sigma_3, \sigma_4) = (1, 1, 0)$,

and reorganize the numerator and denominator:

$$\begin{aligned}
m_1^x \times m_3^x &= \frac{p(x; [12]) p(x; [25])}{p(x; [2]) p(x; [2])} \\
&\propto \frac{\cancel{g_{12}^{11} h_{23}^{10} h_{25}^{10} z_{34}^{00} z_{46}^{00} z_{67}^{00} z_{48}^{00}}}{\cancel{h_{12}^{01} h_{23}^{10} h_{25}^{10} z_{34}^{00} z_{46}^{00} z_{67}^{00} z_{48}^{00}}} \times \frac{\cancel{h_{12}^{01} h_{23}^{10} g_{25}^{11} z_{34}^{00} z_{46}^{00} z_{67}^{00} z_{48}^{00}}}{\cancel{h_{12}^{01} h_{23}^{10} h_{25}^{10} z_{34}^{00} z_{46}^{00} z_{67}^{00} z_{48}^{00}}} \times \frac{g_{23}^{11}}{g_{23}^{11}} \times \frac{h_{34}^{10}}{h_{34}^{10}} \\
&= \frac{g_{12}^{11} g_{23}^{11} g_{25}^{11} h_{34}^{10} z_{46}^{00} z_{67}^{00} z_{48}^{00}}{h_{12}^{01} g_{23}^{11} h_{25}^{10} h_{34}^{10} z_{46}^{00} z_{67}^{00} z_{48}^{00}} \\
&\propto \frac{p(x; [1235])}{p(x; [23])}.
\end{aligned}$$

As $p(x; [23])$, m_1^x and m_3^x have been previously identified, from the above we get the update for $p(x; [1235])$ per Eq. (6), pointing out that indeed $D_2 = \{1, 2, 3, 5\}$ and $F_2 = \{2, 3\}$.

To construct the message m_2^x that factor (2, 3) needs to pass to its own parent (3, 4), we also need the corresponding $p(x; \sigma^{[B_2(\star)]})$, which in the example notation is $p(x; [3])$. But as $B_2 = \{3\}$ is contained in $F_2 = \{2, 3\}$, and this will be the case for all (B_k, F_k) pairs, by assumption Σ_{train} will contain $p(x; [3])$. Therefore, we identified m_2^x .

The steps for (4, 6) and (3, 4) follow identical, if somewhat tedious, reasoning. \square

Proof of Theorem 3.2. Sufficiency follows immediately from the fact that, under Eq. (4) being satisfied, the PR-transformation $\prod_{i=1}^t p(x; \sigma^i)^{q_i}$ is equivalent to

$$\prod_{k=1}^l \prod_{\sigma_{F_k}^v \in \mathbb{D}_k} f_k(x_{S_k}; \sigma_{F_k}^v)^{\sum_{i=1: \sigma_{F_k}^i = \sigma_{F_k}^v} q_i} = \prod_{k=1}^l f_k(x_{S_k}; \sigma_{F_k}^*) \propto p(x; \sigma^*), \quad (7)$$

for all x .

For almost-everywhere necessity, let $z_{kv} := \log f_k(x_{S_k}; \sigma_{F_k}^v)$. Taking the logarithm on both sides of the equality in Eq. (7), we have

$$\sum_{k=1}^l \sum_{\sigma_{F_k}^v \in \mathbb{D}_k} z_{kv} \left(\sum_{i=1: \sigma_{F_k}^i = \sigma_{F_k}^v} q_i \right) = \sum_{k=1}^l z_{k*},$$

which implies

$$\sum_{k=1}^l z_{k*} \left(\sum_{i=1: \sigma_{F_k}^i = \sigma_{F_k}^*} q_i \right) + \sum_{k=1}^l \sum_{\sigma_{F_k}^v \in \mathbb{D}_k \setminus \{\star\}} z_{kv} \left(\sum_{i=1: \sigma_{F_k}^i = \sigma_{F_k}^v} q_i \right) = 0.$$

As no z_{k*} appears in the second term of the expression above, the only way for this equality to hold without $\{q_1, \dots, q_t\}$ satisfying Eq. (4) is if constrains tie together the different z_{k*} . For any reasonable continuous measure by which the parameters of such functions are free to be chosen from (say, as draws of a multivariate Gaussian), this will be a set of measure zero. \square

Discussion. As a corollary it is implied that, similar to the conditions of Theorem 3.1, we need to have at least one train condition σ^i for every possible combination of σ_{F_k} , for each F_k . To see why, imagine if the example of Figure 3 we did not have condition 4, that is, $(\sigma_1, \sigma_2, \sigma_3) = (1, 1, 0)$ is left out. This means that there is nothing to be added in the column f_1^{11} , and the sum $\sum_{i=1: \sigma_{F_1}^i = (1,1)} q_i$ evaluates to 0, implying $g = 1$.

Proof of Theorem 4.1. Vovk et al. [56] introduced a distribution-free procedure for computing prediction intervals with guaranteed finite sample coverage, under the assumption that training and test data are exchangeable. Lei et al. [36] propose a more computationally tractable version that they call the ‘‘split conformal’’ method, and derive a novel upper bound on conformal coverage. We review some fundamental results.

Consider the regression setting with $X \in \mathcal{X} \subseteq \mathbb{R}^d$ and $Y \in \mathcal{Y} \subseteq \mathbb{R}$. We partition the data into two equal-sized subsets $\mathcal{I}_1, \mathcal{I}_2$, using the former for model training and the latter for computing conformity scores. For instance, we may fit a model \hat{f} to estimate $\mathbb{E}[Y | X]$ using samples from \mathcal{I}_1 and consider the score function $S_i = S(x_i, y_i) = |y_i - \hat{f}(x_i)|$ for $i \in \mathcal{I}_2$. Let τ be the q^{th} smallest value in S , with $q = \lceil (n/2 + 1)(1 - \alpha) \rceil$. Define $\hat{C}(x) = \hat{f}(x) \pm \tau$.

Theorem A.1 (Split conformal inference [36]). *Fix a target level $\alpha \in (0, 1)$. If $(x_i, y_i), i \in [n]$, are exchangeable, then for a new sample (x_{n+1}, y_{n+1}) from the same distribution:*

$$P(y_{n+1} \in \hat{C}(x_{n+1})) \geq 1 - \alpha.$$

Moreover, if scores have a continuous joint distribution, then the upper bound on this probability is $1 - \alpha + 2/(n + 2)$.

Tibshirani et al. [54] extend this result beyond exchangeable data by introducing the notion of *weighted exchangeability*. We call random variables V_1, \dots, V_n *weighted exchangeable*, with weight functions w_1, \dots, w_n , if their joint density can be factorized as:

$$f(v_1, \dots, v_n) = \prod_{i=1}^n w_i(v_i) \cdot g(v_1, \dots, v_n),$$

where g does not depend on the ordering of its inputs, i.e. g is permutation invariant. This entails the following lemma.

Lemma A.2 (Weighted exchangeability [54]). *Let $Z_i \sim P_i, i \in [n]$, be independent draws, where each P_i is absolutely continuous with respect to P_1 , for $i \geq 2$. Then Z_1, \dots, Z_n are weighted exchangeable, with weight functions $w_1 = 1$ and $w_i = dP_i/dP_1, i \geq 2$.*

This allows us to generalize the conformal guarantee to weighted exchangeable distributions. Let $\tilde{w}_i(x)$ denote a rescaled version of the weight function, such that weights sum to unity for $i \in [n]$. The original paper does not use the split conformal approach, but we adapt the result below. First, we weight the empirical score function to create the new variable $\tilde{S}_i = S(x_i, y_i) \cdot \tilde{w}_i(x_i)$. Let τ_w be the q^{th} smallest value in \tilde{S} , with q defined as above. Then we construct the weighted conformal band $\hat{C}_w(x) = \hat{f}(x) \pm \tau_w$ for all $x \notin \mathcal{I}_1$.

Theorem A.3 (Split weighted conformal inference [54]). *Fix a target level $\alpha \in (0, 1)$. If (x_i, y_i) , are weighted exchangeable with weight functions $w_i, i \in [n]$, then for a new sample (x_{n+1}, y_{n+1}) :*

$$P(y_{n+1} \in \hat{C}_w(x_{n+1})) \geq 1 - \alpha.$$

Moreover, if scores have a continuous joint distribution, then the upper bound on this probability is $1 - \alpha + 2/(n + 2)$.

Since our causal effects satisfy weighted exchangeability with weight functions given by normalized likelihood ratios, we invoke the result under the regime-wise even partition rule, according to which we enforce representative training and test sets across regimes.

B Elicitation and Testability

As mentioned before, the main result shows that the factorization over X is unimportant for identifiability, which may be surprising. However, it is important to remember that identifiability and testability are two different concepts. While Figure 1(b) has testable implications of conditional independence, testing factorizations may require more intervention levels than the minimal set implied by Theorem 3.1. In particular, if we have a model $p(x; \sigma) \propto \prod_{k=1}^l f_k(x_k; \sigma_k)$, we may be able to identify the model by singleton experiments spanning the range of each σ_i individually, but it does not mean we can falsify this factorization with just this data. In general, our advice for graph construction is akin to any causal modeling exercise: apply independence constraint tests and interaction tests where applicable (see e.g. [48] for an example of nonparametric three-way interaction test), but untestable conditions (under the available data) can be used if there is a sensible theoretical justification for it. This means expert assessment of the lack of direct dependency between an intervention variable and particular random variables; and the split of σ into sets F_k from postulated lack of interactions among intervention variables when causing particular random variables. Although not necessarily always the case, we anticipate that in general this exercise will imply a factorization over the random variables too.

C Covariate Shift Method

As IPW may have large variance, one alternative is to use covariate shift regression [38]. In particular, for each test regime σ^* , we provide a customized estimate of $f_y(x) := \mathbb{E}[Y|X]$.

As before, we combine data from all training regimes $\mathcal{D}^1, \dots, \mathcal{D}^t$, but reweighting then according to (the estimated) $p(x; \sigma^*)$. We propose minimizing the following objective function,

$$\mathcal{L}_y(\theta_y) := \sum_{i=1}^t \sum_{j=1}^{n_i} (y^{ij} - f_y(x^{ij}; \theta_y))^2 w^{ij*},$$

where w^{ij*} is an estimate of $p(x^{ij}; \sigma^*)/p(x^{ij}; \sigma^i)$, and all the training data regimes are weighted equally given that $\sum_{j=1}^{n_i} w^{ij*} = 1$ for all i . As done with the IPW method, this ratio is taken directly from the likelihood function of the deep energy-based model we describe for the direct method.

When generating an estimate $\hat{\mu}_{\sigma^*}$, we just apply the same idea as in the direct method, where samples from the estimated $p(x; \sigma^*)$ are generated by Gibbs sampling, so that we average $f_y(x; \hat{\theta}_y)$ over these samples.

As we are averaging over $f_y(X)$ instead of considering predictions at each realization of X , the main motivation for covariate shift here is to improve on IPW by substituting the use of Y^{ij} as the empirical plug-in estimate of $\mathbb{E}[Y^{ij} | x^{ij}]$ with a smoothed version of it given by a shared learned $f_y(X^{ij}; \theta_y)$. However, in our experiments, this covariate shift method was far too slow when considering the cost over the entire Σ_{test} (as expected, given that the output model is fitted again for every test regime) and did not show concrete advantages compared to the direct method.

D Experimental Details

In this section, we present further experimental details for Section 5, including setup for the datasets (Sachs and DREAM), oracular simulators (Causal-DAG and Causal-IFM), generating ground truth X and Y , model implementation details, and complete training process for our experiments.

D.1 Datasets

Sachs (et al.) dataset. The original Sachs et al. study [45] consisted of 14 different datasets collected under different compound perturbations in single-cell systems measured by 11 protein/lipid concentrations. Perturbations can be described in terms of binary intervention variables, labeled by the associated compound. For instance, condition *pma* describes the introduction or not of phorbol 12-myristate 13-acetate. Among all perturbations, *pma* and *b2camp* are entangled with *cd3cd28* (this means, for instance, that *pma* = 1 or *b2camp* = 1 imply *cd3cd28off* = 1). Hence, we ignore these two experimental setups, and all remaining datasets are collected under *cd3cd28* = 1 so that it can be considered as an implicit condition not modeled explicitly with a separate intervention variable.

Other conditions implying unresolved entanglements were not considered, in particular the uses of *icam-2* and *ly294002*. The remaining datasets are listed in Table 1. Assumptions about each intervention targeting a single protein in the network are taken from [45]. In summary, the original Sachs et al. data used to train the simulator contains samples from 5 (1 “baseline” plus 4 “perturbed”) different regimes, and each data sample has 11 variables.

Since each intervention is considered as a binary value (0 for no perturbation and 1 for perturbation), this gives us a total of $2^4 = 16$ combinatorial possibilities, with 5 in Σ_{train} . Hence, we need a way of establishing a (synthetic) ground truth for the $16 - 5 = 11$ possible test conditions, which we explain in Section D.2.

DREAM dataset. The DREAM challenges include a series of problems for causal inference in protein networks [22]. We generate data based on a known *E. coli* sub-network with 10 nodes, and consider that each random variable X_i has a corresponding interventional variable σ_i . We use the GeneNetWeaver simulator⁴ to generate this data, under "InSilicoSize10-Ecoli1" from the "DREAM3_In-Silico_Size_10" task and there is no further data selection process as in the Sachs case. The simulation is based on a series of predefined ODEs and SDEs. For each data regime, a single data sample is collected with a random seed initialization with an otherwise exact similar simulation setting for that particular regime. Following [55],

⁴<https://gnw.sourceforge.net>

Table 1: Details for the Sachs et al. datasets used for our first batch of intervention generalization experiments. Data files can be downloaded from the website of the original reference [45], with the name described below. Column *Target X node* describes the theoretical direct connection (as given by [45]) between the perturbation and 11-dimensional system described by a vector of 11 random variables X , with condition $cd3cd28$ always present and affecting all variables, and hence interpreted as a targeting none. As described in Section D.2, we encode each regime as a 11-dimensional binary vector, and display them in the last column. A julia notebook exemplifying the pre-processing of this data and a Julia script outlining a complete pipeline of batch simulated experiments comparing methods is provided in the supplementary material.

File name	Target X Node	Data Regime	Corresponding σ
cd3cd28.xls	None (background condition)	Regime 0	[0, 0, 0, 0, 0, 0, 0, 0, 0, 0, 0]
cd3cd28+aktinhib.xls	Variable 7	Regime 1	[0, 0, 0, 0, 0, 0, 1, 0, 0, 0, 0]
cd3cd28+g0076.xls	Variable 9	Regime 2	[0, 0, 0, 0, 0, 0, 0, 0, 1, 0, 0]
cd3cd28+psitect.xls	Variable 4	Regime 3	[0, 0, 0, 1, 0, 0, 0, 0, 0, 0, 0]
cd3cd28+u0126.xls	Variable 2	Regime 4	[0, 1, 0, 0, 0, 0, 0, 0, 0, 0, 0]

we gather the data sample once it reaches its equilibrium state and repeat this process as many times as the sample size required. In summary, this provides us with a dataset consisting of 11 (1 baseline plus 10 perturbation) regimes. As we are interested in combinations of 10 binary indicator variables σ_i , not directly provided in the original DREAM simulator, we had to create our own ground-truth synthetic model based on samples from the 11 regimes we can obtain from DREAM.

D.2 Oracular Simulators

Both Sachs and DREAM come with a ground truth DAG (either defined by expert domain knowledge or motivated by physical systems dynamics). We used each of the DAGs to construct the associated IFMs. To further explain: in a DAG, the joint probability distribution can be factorized based on the local Markov condition [32], where a single factor is defined by a vertex and its parents; this suggests are least one IFM, with the factorization following from interpreting each child-parents factor as a black-box (i.e., not normalized by the child) positive function of these variables. Graphically, this is known as the *moralization* step of “marrying the parents” followed by the dropping of directions in order to create an undirected Markov network [32]. We use this to define a factor graph model without stating that this would be the best representation for the corresponding data. It relaxes the DAG assumption (i.e., it removes some of the independence constraints encoded in the DAG) and could be refined by adding other constraints (such as breaking the factors into products of reduced sets of variables), which we do not attempt. See Figure 8 for an example with the Sachs et al. model. Approaches such as [1] could be used to refine this structure, if so desired.

Given two theoretical constructions and the respective parameterizations they use, this suggests *two* ways of building ground-truth simulator models to generate ground truth data X , which we now explain.

Common to both ground-truth simulators is the fitting of a postulated causal structure to real data (either Sachs or DREAM). Prior to fitting, we scale the data of each study so that the respective “merged empirical distributions”, defined by taking the union of all respective datasets collected under all available training regimes, have empirical mean of zero and empirical variance of 1 for each measured random variable. This does not mean any given variable in any given training regime will have zero empirical mean and unit variance, but pragmatically it helps to control having variables with disparate scales. For the Sachs data, we also take the logarithm of each random variable prior to standardization.

D.2.1 Causal DAG Ground-Truth

The first ground-truth simulator is implied by the respective causal DAG model. The DAG for each study are shown in Figures 8(a) and 9(a). The factorization comes from the structure of the DAG and can be rewritten as follows:

$$p(x; \sigma) = \prod_{k=1}^l p(x_k \mid \mathbf{pa}(x_k); \sigma_{F_k}), \quad (8)$$

where, l is the total number of random variables, $p(x_k \mid \mathbf{pa}(x_k); \sigma_{F_k})$ is the conditional density function for x_k , σ_{F_k} is the regime indicator subvector for the intervention variables which are parents of x_k in the DAG, and $\mathbf{Pa}(x_k)$ refers to the random variables which are parents of x_k .

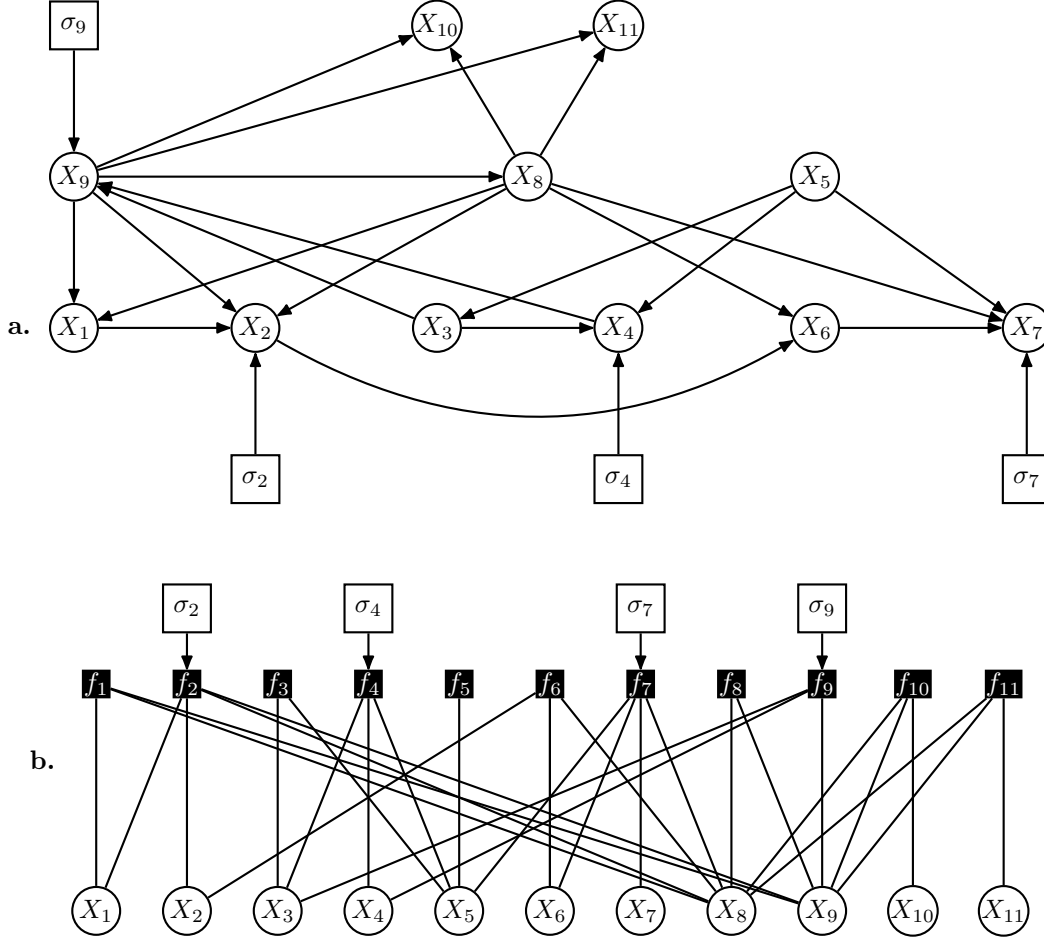


Figure 8: Causal structures used for building the synthetic ground-truth models for the Sachs et al. [45] data. The name of the random variables are *CD3CD28off*, *ICAM-2*, *Akt-inhibitor*, *G0076*, *Psitectorigenin*, *U0126*, *LY294002*, *PMA*, *B2camp*, with more details given in the companion Julia notebook. (a) A directed acyclic graph (DAG) for the Sachs et al. process, with intervention vertices representing intervention variables. (b) The interventional factor graph, inspired by the DAG, which we use in our synthetic ground-truth simulator. This is done by creating a factor for each child and parent set from the postulated DAG. These independence models are not equivalent. The point is *not* to provide an exact model, but to build a synthetic ground truth with parameters calibrated by real data instead of arbitrarily sampled, and with independence constraints and factorizations that do not contradict a given expert assessment (as the factor graph contains *fewer* independence assumptions than the DAG, not more).

For parameterizing the causal DAG model family, we assume a heteroscedastic conditionally Gaussian formulation. This can be represented by the equation

$$X_k = f_k(\mathbf{pa}(X_k), \sigma_k) + g_k(\mathbf{pa}(X_k), \sigma_k) \times \epsilon_k, \epsilon_k \sim \mathcal{N}(0, 1).$$

Here, each f_k and g_k are multilayer perceptrons (MLPs) with 10 hidden units and the role of σ_k is just a switch: for each value of σ_k , we pick one independent set of parameters for the MLP mapping $\mathbf{pa}(X_k)$ to the real line. To learn the parameters in functions f_k and g_k , maximum likelihood is used. Further details are provided in the companion Julia code.

D.2.2 IFM Ground-Truth

The second simulator is the causal IFM. The factorization comes from the structure of the DAG, using the moralization criterion described in the previous section. Figures 8(b) and 9(b) show the respective

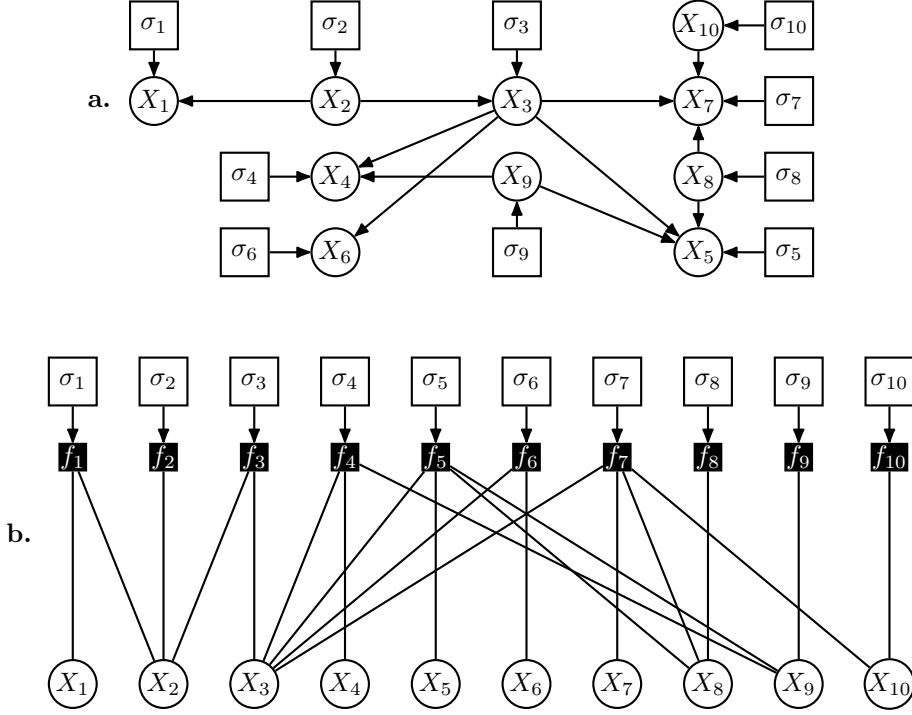


Figure 9: The DREAM structural assumptions, following a process analogous to the Sachs et al. case described in Figure 8.

IFM graph structure. This results in the following factorisation form:

$$p(x; \sigma) \propto \prod_{k=1}^l f_k(x_{\{k\}} \cup \mathbf{pa}(x_k); \sigma_{F_k}), \quad (9)$$

where $\mathbf{pa}(x_k)$ comes from the respective theoretical causal DAG case, with F_k given accordingly by k . To learn the causal IFM simulator, we use pseudo-likelihood and assign each factor again to a black-box MLP of 15 hidden units where the corresponding σ_{F_k} is a switch between independent sets of parameters within each factor. We additionally perform a discretization step for variable X_i by collecting all data and doing uniformly binning it in 20 bins, so that it is faster to compute the conditional normalizing constants⁵ for each term in the pseudo-likelihood objective function.

To sample from the learned IFM, so that we can numerically compute quantities such as μ_σ , we use Gibbs sampling.

D.3 Generating Ground-Truth Population Models and Data

Generating ground truth data, either for numerically computing population quantities by Monte Carlo or as a generator of training data, includes the following steps: (1) learning simulators, (2) generating ground truth X and (3) generating ground truth Y .

Learning simulators. The first step involves learning the simulators: with the Sachs et al. data, we use 5 data regimes as the training data for the simulator (1 baseline regime and 4 interventional); and with DREAM data, we use 11 data regimes as the training data for the simulator (1 baseline regime and 10 interventional). As described above, two simulators are built for each of the two studies.

Generating ground-truth system X . Since each intervention is considered as a binary value (0 for no intervention and 1 for with intervention), with the training dataset of 5 data regimes in Sachs, this

⁵While it is theoretically possible to use continuous variables and automatic differentiation through a quadrature method that computes each univariate integral for each term in the pseudo-likelihood, this is still far too slow in practice. The discretization level chosen for these examples are fine enough so that it does not appear to affect the predictive performance of the $p(y | x)$.

gives us a total of $2^4 = 16$ combinatorial possibility regimes; as for the DREAM case, we have in total of 11 regimes, which means that the complete space Σ has $2^{10} = 1024$ combinations. To simplify the computation of the benchmark, we are interested in the "one-to-double knockdown" scenario and hence generate a total of 56 regimes ($= \frac{10 \times 9}{2} + 11$).

The original training datasets for both simulators are discarded and we now consider the simulator as the oracle for any required training set and population functionals. In particular, for each regime, we generate 25,000 samples to obtain a Monte Carlo representation of the ground-truth respective population function $p(x; \sigma)$.

Generating ground-truth outcome processes Y . For outcome variables Y from which we want to obtain $\mu_{\sigma^*} := \mathbb{E}[Y; \sigma^*]$ for given test regimes σ^* , we consider models of the type $Y = \tanh(\lambda^\top X) + \epsilon_y$, with random independent normal weights λ and $\epsilon_y \sim \mathcal{N}(0, v_y)$. λ and v_y are scaled such that the ground truth variance of $\lambda^\top X$ is a number v_x sampled uniformly at random from the interval $[0.6, 0.8]$, and set $v_y := 1 - v_x$.

For each of the four benchmarks (i.e., based on either the Sachs et al. data or DREAM data, with either a DAG model-based ground-truth or an IFM-based ground truth), we generate 100 random vectors λ . The point of these 100 problems is just to illustrate the ability to learn (noisy) summaries of X , or general downward triggers or markers predictable from X under different conditions. When generating Y from X , we keep a single sample for X . We then generate an unique sample for each of the 100 Y variations given the same X data.

Generating training data. For training our models, we additionally generate 5000 samples for the observational regime (baseline) and 500 samples for each of the remaining 4 experimental conditions (Sachs) and 10 experimental conditions (DREAM). To map from X to Y , we use the model described above.

D.4 Implementation Details

We now describe the implementation details, which are also detailed in the companion source code.

- **Blackbox Model:** We use the Julia wrapper of XGBoost⁶. In practice, given how sparse Σ_{train} is in the space Σ of possible combinations, this is hardly more effective than linear regression (results not shown);
- **Causal DAG:** We set each heteroscedastic MLP model with a hidden dimension of 10 and this is the same setting we used for the Causal DAG simulator. This gives this competitor much advantage in the benchmarks generated by DAGs, as following a parametric Gaussian with additive error structure is already substantive information to be exploited;
- **IFM:** We implemented the IFM model with a combination of neural factors, where each factor is determined by the DAG structure and each MLP has 25 hidden units. Note that the number of hidden units does not match the one used to generate the data.

E Further Experimental Results

E.1 Further Experimental Metrics

We present a series of further experimental results in numerical form based on the following metrics: (1) *proportional root mean squared error* (pRMSE): the average of the squared difference between the ground truth Y and estimated \hat{Y} , where each entry is further divided by the ground truth variance of the corresponding Y ; and (2) *rank correlation* (rCOR): the Spearman's ρ between the ground truth vector μ_{σ^*} for all entries in Σ_{test} , and the corresponding estimated vector (see Table 2⁷).

E.2 Binomial Tests

We present results from a series of one-sided binomial tests to determine whether models significantly outperform the black box baseline (see Table 3).

⁶<https://juliapackages.com/p/xgboost>.

⁷The IFM-3 results are omitted from Tables 2 and 3, as the method does not convergence in a reasonable time.

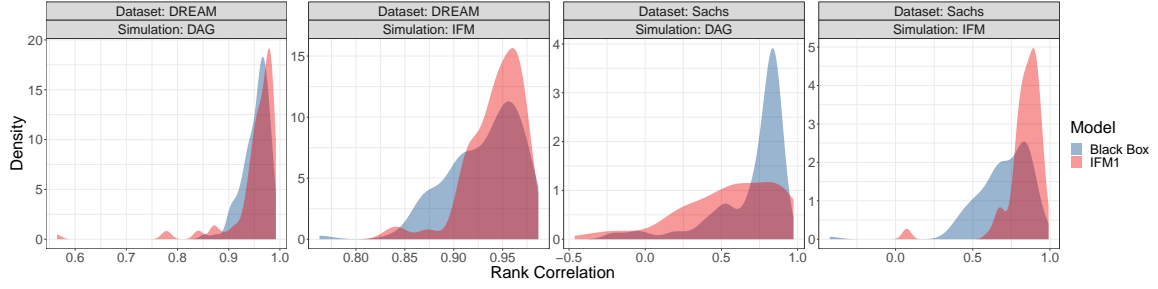


Figure 10: Overlapping density plots showing average rank correlation between true treatment effects and those predicted by the black box model and IFM1, respectively. Ideal performance is a point mass on 1.

	Sachs		DREAM	
	<i>Causal-DAG</i>	<i>Causal-IFM</i>	<i>Causal-DAG</i>	<i>Causal-IFM</i>
	pRMSE	pRMSE	pRMSE	pRMSE
Blackbox	0.043	0.414	0.025	0.174
Causal-DAG	0.014	0.408	0.017	1.337
IFM-1	0.105	0.168	0.022	0.185
IFM-2	0.051	0.111	0.107	0.769
IFM-3	0.123	0.175	–	–
	rCOR	rCOR	rCOR	rCOR
Blackbox	0.696	0.701	0.953	0.930
Causal-DAG	0.873	0.405	0.972	0.502
IFM-1	0.546	0.835	0.952	0.942
IFM-2	0.673	0.821	0.865	0.737
IFM-3	0.503	0.811	–	–

Table 2: Experimental results for Sachs and InSilicoSize10-Ecoli1 datasets for our interventional generalization experiments. The values are correspond to the average of 100 Y problems.

Table 3: P-values from a series of one-sided binomial tests against the null hypothesis that models perform no better on average than the black box model. Significance at $\alpha = 0.05$ is indicated with one asterisk, and $\alpha = 0.001$ with two.

Data	Simulation	DAG	IFM1	IFM2	IFM3
DREAM	Causal-DAG	< 0.001**	0.044*	1	NA
DREAM	Causal-IFM	1	0.972	1	NA
Sachs	Causal-DAG	< 0.001**	1	0.998	1
Sachs	Causal-IFM	0.956	< 0.001**	< 0.001**	< 0.001**